Study on Interaction Mechanism of Different Atomic Ratio of Neodymium, Arsenic and Iron

Juncheng Mao
Guizhou University
Run Huang
Guizhou University
Chenghui Fu
Guizhou University
Xiaodong Lv
Chongqing University
Lihua He
Guizhou University
Jinzhun Zhang (jzzhang@gzu.edu.cn)
Guizhou University

Research Article

Keywords: neodymium, arsenic, iron, compound, heterogeneous nucleation

Posted Date: November 24th, 2020

DOI: https://doi.org/10.21203/rs.3.rs-107056/v1

Version of Record: A version of this preprint was published at Scientific Reports on February 19th, 2021.
See the published version at https://doi.org/10.1038/s41598-021-83698-9.

Study on Interaction Mechanism of Different Atomic Ratio of Neodymium, Arsenic and Iron

Juncheng Mao [1,2], Run Huang [1,2,*], Chenghui Fu [1,2], Xiaodong Lv [3], Lihua He [1,2] and Jinzhu Zhang [1,2,*]

1 School of Materials and Metallurgy, Guizhou University, Guiyang 550025, PR China
2 Guizhou Province Key Laboratory of Metallurgical Engineering and Energy Process Saving, Guiyang 550025, PR China
3 College of Materials Science and Engineering, Chongqing University, No.174 Shazheng Street, Shapingba District, Chongqin, 400044, PR China
* Correspondence: rhuang@gzu.edu.cn, jzzhang@gzu.edu.cn

Abstract: In this study, neodymium and arsenic were sealed into industrial pure iron cylinders at a temperature of 1223 K for 50 h. The interaction mechanism of the Nd-Fe-As system at various atomic ratios was investigated by optical microscopy, X-ray diffractometry, and scanning electron microscopy. Binary compounds $Fe_{12}As_5$, NdAs, Fe_2As, and $Fe_{17}Na_2$ were the main products formed, with traces of NdFeAs compounds. In addition, at high temperatures, As content affected the diffusion of Fe atoms; the diffusion of Fe increased with an increase in the atomic ratio. Furthermore, the diffusion ability of Nd was weaker than that of As. The major diffusion mechanism of Nd was through the Fe atomic vacancy mechanism. As mainly bind to Fe to form Fe and As compounds. The formation of ternary compounds was confirmed by laboratory experiments and mismatch calculations.

Keywords: neodymium; arsenic; iron; compound; heterogeneous nucleation

Introduction

Rare earth elements (including 15 lanthanide elements, scandium, and yttrium[1-3] in the third subgroup of the periodic table) are widely used for the purification, metamorphosis, and alloying of metals[4-5]. The unsaturated outer electronic layer of rare earth elements is considered as a special form of new materials, which can burst out a variety of electron energy levels and exhibit high "vitality" in its external performance. In addition, rare earth elements are regarded as a treasure of new materials because of its unique electrical and magnetic properties. Arsenic, as a deleterious element commonly occurring in steel, leads to the segregation of As, grain boundary segregation, and oxidation during solidification, which deteriorate the thermoplastic, tempering brittleness, hot workability, and mechanical properties of steel[6]. Rare earth elements can react with As (with a low melting point) to form compounds with high melting point because of their active chemical properties, thus improving the thermoplastic and mechanical properties of steel.

According to the iron-neodymium (Fe-Nd) binary phase diagram [7], the stable compounds that can be formed between Fe and Nd include $Fe_{17}Nd_2$ and Fe_2Nd, and according to the Fe-As binary phase diagram, the stable compounds that can be formed between Fe and As include Fe_2As, Fe_3As_2, FeAs, and $FeAs_2$[8]. Generally, the maximum solubility of As in Fe is approximately 10% at 1113 K[9]. However, the solubility decreases with a decrease in temperature and reduces to below 5% at room temperature[10-12]. For Re-Fe-As ternary system, the main products including $REFe_4As_{12}$, $REFe_2As_2$ (RE=La, Nd, Sm) have been widely reported. Different atomic ratios of cerium (lanthanum), Fe, and As form the ternary compound $RE_{12}Fe_{57.5}As_{41}$ (RE=La, Ce) and FeAs at 1173 K[13-14], whereas the Re-Fe-As ternary system forms $La_{10}Fe_{50}As_{40}$[15] at 1223 K. In recent years, one of products of RE-Fe-As ternary system named $EuFe_2As_2$[16-20] has attracted significant attention. Xie[21]and Fu[22] investigated the interaction of Nd-Fe-As system at high temperatures and found that the formation of the ternary compound NdFeAs depends on the formation of NdAs and $FeAs_2$.

Therefore, in this study, a certain quality of Nd and As were sealed in a cylinder block, which was specially processed using industrial pure Fe by melting, infiltration, and diffusion. The interaction between Nd, Fe, and As at high temperature and the mechanism for the generation of ternary compounds was investigated using metallographic microscope, scanning electron microscope (SEM), and X-ray diffraction (XRD). The generation of ternary compounds was partly confirmed by calculations and laboratory experiments.

Materials and Methods

Figure 1 shows the barrel-shaped cylinder composed of industrial pure Fe; its principal chemical composition (mass fraction) is as follows: 0.002% C, 0.02% Mn, 0.006% P, 0.004% S, 0.005% Al, and 99.95% Fe. Nd metal block (purity>99.9%) and As block (diameter<1 mm, see Table 1) were filled into the industrial pure Fe cylinder block at various atomic ratios (1:1,1:2,1:3), the screw plug was welded by arc welding, and a high temperature sealant was applied to the weld to ensure it is properly sealed. Subsequently, the industrial pure Fe cylinder block was placed in a closed tube vacuum furnace and heated under high purity argon SRJK-2-9 atmosphere. The experimental heating process is shown in Table 2, and it depended on the vapor pressure of As. After the heating process, the temperature of the furnace was reduced to room temperature(30°C). Subsequently, argon flow into the furnace was stopped and the cylinder sample was taken out. Then, the outer side of the cylinder block was marked away from its bottom (at a distance of 16 mm); in the radial direction, it was sawed and divided into two parts, one of which was processed into metallographic samples and the other part was used for XRD analysis. The phase composition of the samples was analyzed using a PHILIPS X'-Pert PRO diffractometer, and the test parameters are as follows: Copper target, λ=0.154056 nm, 40 kV operating voltage, 2°/min scanning speed.

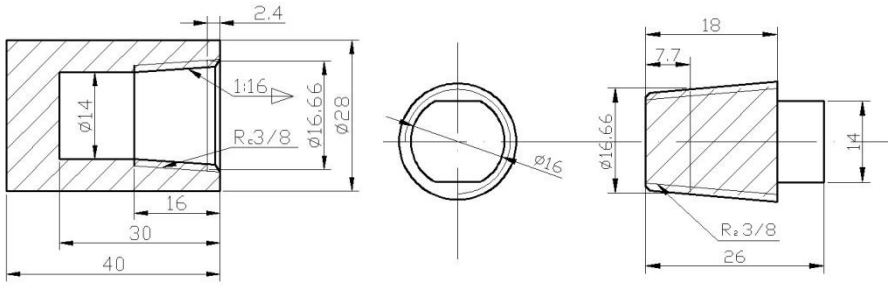

Figure 1. Schematic of the barrel-shaped cylinder and the screw plug.

Table 1. Masses of Nd and As and the atomic ratio of Nd:As for sample preparation.

Sample	Atomic ratio	Nd/g	As/g	T/K	t/h
1#	1:1	6.5814	3.4185	1223	50
2#	1:2	4.9014	5.0985	1223	50
3#	1:3	3.9089	6.0911	1223	50

Table 2. Experimental heating process.

Experimental heating process
$\text{Room temperature} \xrightarrow{2h} 773K \xrightarrow{10K/10min} 923K \xrightarrow{10K/20min} 983K \xrightarrow{10K/30min} 1023K \xrightarrow{10K/1h} 1073K \xrightarrow{10K/2h} 1123K \xrightarrow{10K/5h} 1173K \xrightarrow{10K/6h} 1223K(50h)$

Results

Metallographic Analysis

Figure 2 shows the metallographic images of the samples at various atomic ratios under an optical microscope. At a constant heating temperature and holding time, three types of contrast (grayish, gray, and black) were observed at different atomic ratios. The grayish part indicates the collective part of the cylinder, most of which was the industrial pure Fe, the gray part has a higher proportion of As, and the black part has a higher proportion of Nd. Figure 2(a) shows the neighboring area of the cylinder block, which indicates that the entire area was divided into two different parts: the cylinder matrix on the left and the core component on the right. In addition, inhomogeneous granular structures were formed at all atomic ratios (the right area), and they contained the same white liner as the cylinder matrix. With an increase in the atomic ratios, the symmetry of the entire granular structure increased and then decreased. In addition, with an increase in the diffusion of the grayish area, the diffusion moved farther away from the edge, which consequently reduced the diffusion. Particularly, with a decrease in the distance between the gray area and the edge of the boundary, the proportion of the gray area reduced. At high temperatures, the Fe atom diffused into the core area of the sample, while the Nd atom diffused into the matrix area, and the Fe and As atoms diffused together, and consequently, Fe atoms gradually formed a circular structure.

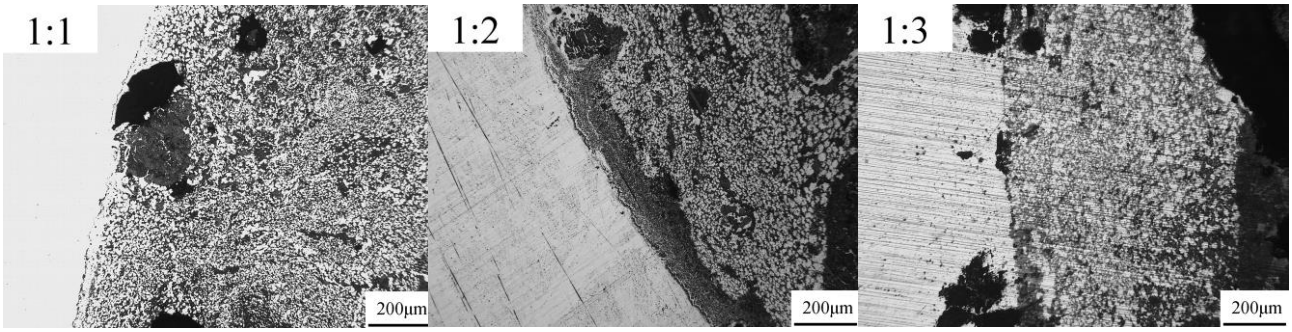

(a)

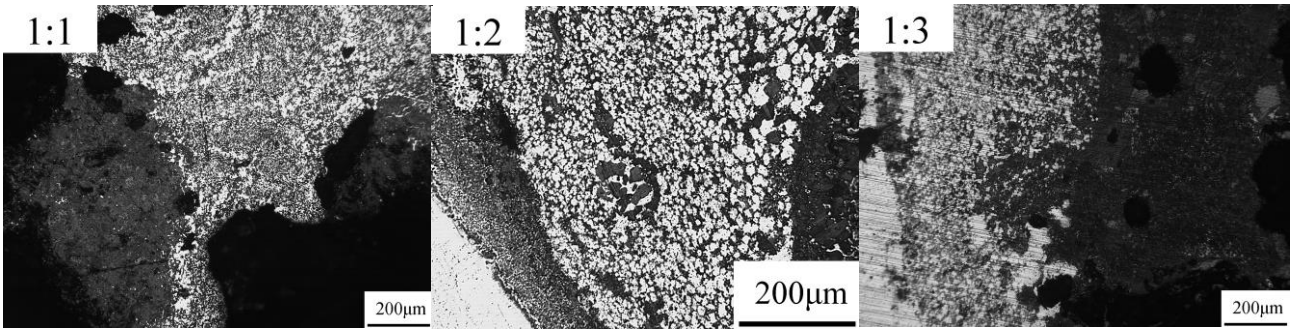

(b)

Figure 2. Metallographic pictures of atoms at different atomic ratio, (a) Pictures of the cylinder block's neighboring area, (b) Pictures around its core area.

Phase Analysis

For the phase analysis, the sample from the core area was ground in a mortar into a powder. Subsequently, the phase of the samples was characterized by XRD analysis, as shown in Figure 3. The main diffraction peaks observed in the XRD spectra could be attributed to the formation of five types of compounds ($Fe_{12}As_5$, Fe_2As, NdAs, $Fe_{17}Nd_2$, and α-Fe) in the ternary system of the high-temperature fusion samples. When the atomic ratio of Nd and As was 1:1 and 1:2, the intensity of the diffraction peaks was stable. During the experiment, As sublimed at high temperatures, while the highly reactive Nd reacted with As. Consequently, the amount of compounds (NdAs) increased.

As the experiment progressed, a small amount of As diffused into the external matrix of the cylinder block, and Fe diffused to its core area and reacted with As, forming As compounds (Fe_2As).

XRD spectra of Nd-Fe-As powder compounds in the ternary system were not found in relevant

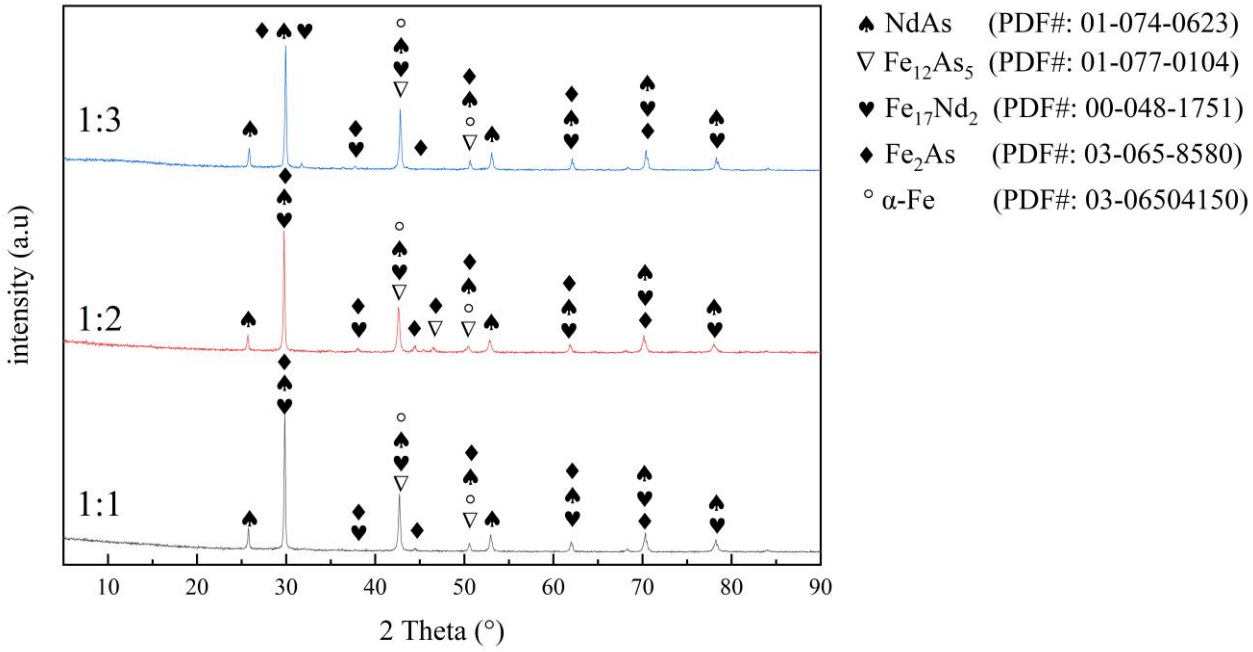

Figure 3. X-ray diffraction spectra of the samples at different atomic ratio.

literature. However, the energy dispersive spectroscopy (EDS) analysis suggests the formation of the ternary compounds (NdFeAs).

SEM analysis was carried out on the reduced sample, and EDS analysis was employed to analyze the image at different contrasts. As shown in Figure 4, the samples are mainly distributed in four types of contrast phase (black, dark gray, light gray, and white), which are identified by A, B, C, and D, and each contrast phase tissue was investigated using EDS analysis; the results are shown in Table 3. The microstructure of the black, dark gray, and light gray contrast had an irregular shape. In addition, the gray and light gray components were mainly composed of Nd and As, combined with the XRD spectra of Nd and As, this result indicates that the contrast phase structure was a NdAs crystal structure, whereas the black contrast phase structure was mostly saturated As α-Fe solid solution.

As discussed above, the products of Nd and As at different atomic ratios (1:1, 1:2, 1:3) contained $Fe_{12}As_5$, Fe_2As, NdAs, and $Fe_{17}Nd_2$ in all the ternary systems. However, the amount of different phases changes with an increase in the atomic ratios, and the various contrast phase structures show a symbiotic relationship.

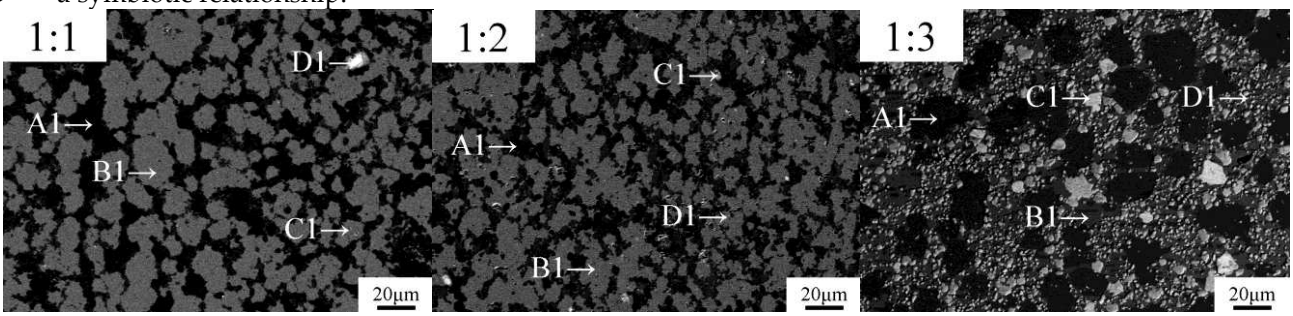

(a) (b) (c)

Figure 4. Backscattered electron maps of the sample at various atomic ratios (a) 1:1, (b) 1:2, (c) 1:3.

Table 3. EDS analysis results of different atomic ratio samples (at/%).

Positions	Nd	As	Fe	Positions	Nd	As	Fe	Positions	Nd	As	Fe
A1	45.39	48.93	5.69	A1	44.32	43.34	12.34	A1	0.25	9.07	90.68
B1	35.14	42.24	22.63	B1	39.98	39.33	20.69	B1	39.39	42.34	18.27
C1	21.11	21.89	57.00	C1	20.79	27.75	51.46	C1	50.79	46.96	2.24
D1	2.27	11.21	86.52	D1	8.50	18.87	72.63	D1	0.74	8.55	90.72

Diffusion analysis of samples

Figure 5 shows the line-scanning atlas analysis of the transition areas of Nd and As at different atomic ratios. According to the graph, the three elements (Nd, Fe, As) were in a continuous distribution in a banded gradient. In addition, the amount of Nd in the white contrast region was significantly higher than that in other regions. Furthermore, the amount of Fe in the black contrast region was the highest, and As existed in all the contrast phases.

During the experiment, Fe diffused into the cylinder block, whereas the diffusion activation energy of As was lower than that of Fe[23]. In addition, As diffused via the formation of Fe and As compounds, and Nd diffused via its vacancy mechanism and the formation of the Fe and As compounds. Because the chemical potential of Nd increased with an increase in its content, and the solubility of As was maintained at 10% during experimental temperature, vacancies were produced during the sublimation process. The interaction between As and Nd produced NdAs compounds, and the remaining Nd and Fe formed $Fe_{17}Nd_2$ compounds to fill the vacancies. In addition, Fe vacancies were formed by thermal vibration; consequently, these vacancies provided a condition for the diffusion of Nd[24]. Furthermore, the grain size gradually decreased, thus increasing the grain boundary area. Simultaneously, the grain boundary vacancies increased accordingly. The combined effect of the generated vacancies, the Nd-generated solute-vacancy compounds, and the enhancement of the thermal diffusion rate leads to the segregation of Nd at the grain boundary.

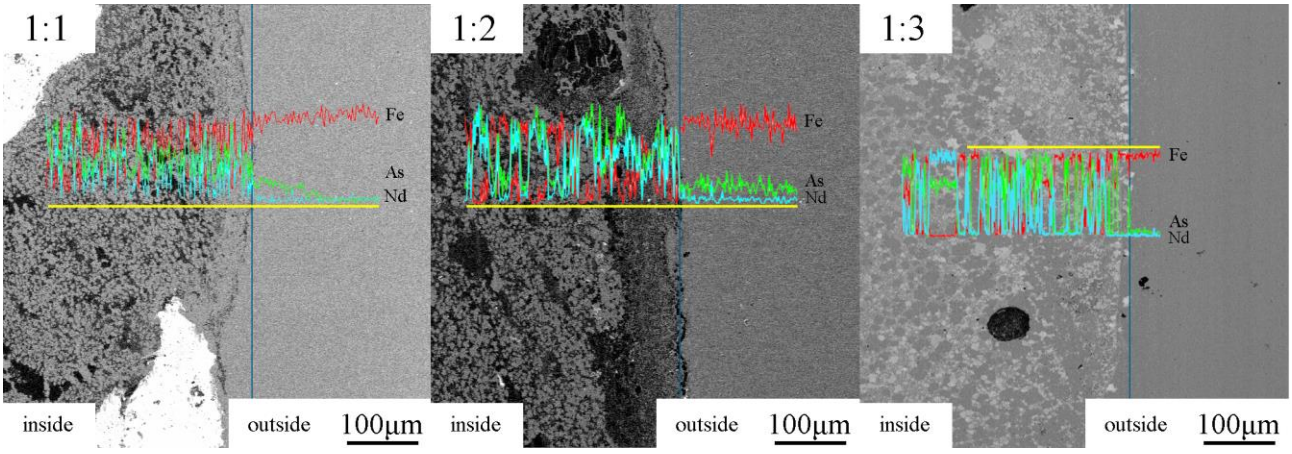

Figure 5. Sweep spectrum of the edge line of the cylinder samples at different atomic ratio.

Planar mismatch calculation and analysis

According to the planar mismatch theory, the calculation result of the mismatch of two planes should be less than 6% to achieve good heterogeneous nucleation; heterogeneous nucleation is expected to occur if the mismatch is greater than 12%. The planar mismatch can be calculated using Equation (1)[25].

$$\delta_{(hkl)_n}^{(hkl)_s} = \frac{1}{3}\sum_{i=1}^{3}\left[\frac{\left|d_{[uvw]_s}^{i}\cos\theta - d_{[uvw]_n}^{i}\right|}{d_{[uvw]_n}^{i}}\right] \times 100 \quad (1)$$

where δ is the average of the three mismatches between the $(hkl)_s$ and $(hkl)_n$ planes; $d_{[uvw]_s}$ and $d_{[uvw]_n}$ is the interatomic spacing along $[uvw]_s$, and $[uvw]_n$ respectively; and θ is the angle between two corresponding direction.

The atom matching diagram of the surface between the $Fe_{12}As_5$ (0001) and NdAs (111) planes is illustrated in Figure 6 and Figure 7. The former is indicated by yellow circles and the latter is indicated by green circles. The crystal parameters involved in the calculations are listed in Table 4[26], and the specific calculation data are shown in Table 5. The calculation results of the two mismatched planes was 17.86%, indicating that $Fe_{12}As_5$ cannot be used as the effective heterogeneous nucleation core in the formation NdAs.

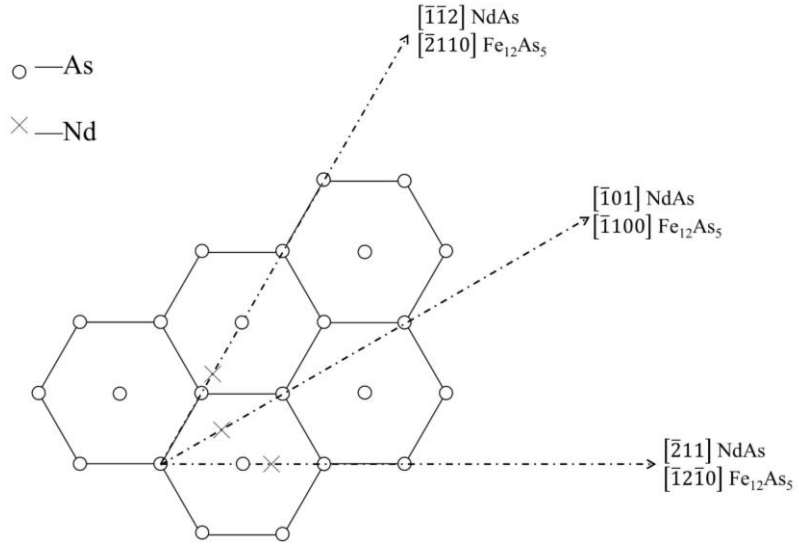

Figure 6. Crystallographic relationships of the $Fe_{12}As_5$ (0001) and NdAs (111) planes.

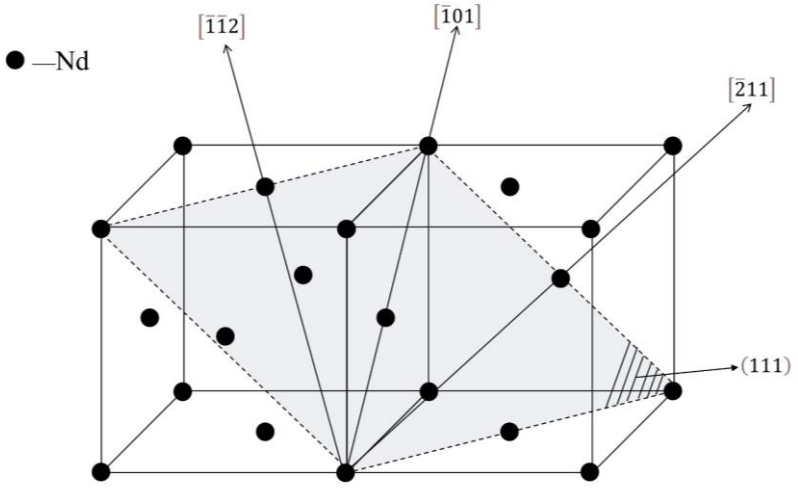

Figure 7. Diagram of plane and crystal direction of NdAs (111).

The calculation results of the mismatch are listed in the table 6. The mismatch between Fe_2As and NdFeAs was 8.33%, indicating the high probability for Fe_2As to effectively act as the heterogeneous nucleation cores for the formation of ternary NdFeAs compound.

Table 4. Crystallographic parameters of possible compounds of Nd and As in steel.

Compounds	Crystal System	Lattice Parameters (25°C, nm)		
		a_0	b_0	c_0
$Fe_{12}As_5$	hexagonal	0.6786	-	1.6301-
NdAs	cubic	0.5987	-	-
Fe_2As	tetragonal	0.3632	-	0.5981
$Fe_{17}Nd_2$	hexagonal	0.8574	-	1.2464
NdFeAs	tetragonal	0.39655	-	0.8575

Table 5. Calculation details of the lattice between $Fe_{12}As_5$ and NdAs compounds.

Interface	$(0001)Fe_{12}As_5//(111)NdAs$		
$(hkl)_s$	$[\bar{1}2\bar{1}0]$	$[\bar{1}100]$	$[\bar{2}110]$
$(hkl)_n$	$[\bar{2}11]$	$[\bar{1}01]$	$[\bar{1}\bar{1}2]$
$d[hkl]_s$	0.6786	1.1745	0.6786
$d[hkl]_n$	0.7331	0.4233	0.7331
θ	0	0	0
$d[hkl]_s \cdot \cos\theta$	0.6786	1.1745	0.6786
δ(%)	64.11		

Table 6. Calculated planar lattice misfits among crystal faces of Nd-Fe-As inclusions.

Interface	δ(%)	Effectiveness
$(0001)Fe_{12}As_5//(111)\,NdAs$	64.11	Least Effective
$(0001)Fe_{12}As_5//(0001)Fe_{17}Nd_2$	48.82	Least Effective
$(0001)Fe_{12}As_5//(112.162)NdFeAs$	19.95	Least Effective
$(001)NdAs//(001.647)Fe_2As$	22.96	Least Effective
$(111)NdAs//(0001)Fe_{17}Nd_2$	109.04	Least Effective
$(001)NdAs//(002.162)NdFeAs$	28.38	Least Effective
$(111.647)Fe_2As//(0001)Fe_{17}Nd_2$	37.21	Least Effective
$(001.647)Fe_2As//(002.162)NdFeAs$	8.33	Very Effective
$(0001)Fe_{17}Nd_2//(112.162)NdFeAs$	18.36	Least Effective

Conclusions

(1) When the atomic ratios of Nd and arsenic were between 1:1–1:3 at a maximum temperature of 1223 K for 50 h, $Fe_{12}As_5$, Fe_2As, NdAs, and $Fe_{17}Nd_2$ were formed. In addition, with an increase in the atomic ratios of Nd and As, the formation of the NdAs compounds decreased and the formation of Fe_2As compounds increased (Fe_2As was generated during the diffusion of As toward the cylinder block).

(2) In the ternary system (Nd-Fe-As), the diffusion of Fe was dependent on the amount of As. In addition, the Fe atom diffused toward the core of the cylinder block, and its amount decreased with

increase in the depth of its diffusion. Furthermore, with an increase in the proportion of Nd and As, the diffusion of As into the external matrix of the cylinder increased.

(3) The EDS spectra suggest the formation of ternary compounds (NdFeAs), and the mismatch calculation indicated that the Fe_2As can act as effective heterogeneous nucleation cores for the formation of ternary compounds (NdFeAs).

References

1. Zhang, F., Li, Y.; Li, X. Current status of rare-earth resources development and utilization at home and abroad and suggestions for rare-earth management in China. *Modern Mining*. **12**, 11-14. https://dx.doi.org/10.3969/j.issn.1674-6082.2018.12.003 (2007).
2. Dutta, T., Kim, K. H., Uchimiya, M., Kwon, E. E., Jeon, B. H. & Deep, A. *et al*. Global demand for rare earth resources and strategies for green mining. *Environmental Research.* **150**, 182-190. https://doi.org/10.1016/j.envres.2016.05.052 (2016)
3. Zhang, Y., Liu, C. S., Gao, L. F., Zhang, Z. G. & Zhang, P. Marine authigenic deposits mineral-new fields for the development for the development of rare-earth resources. *Advanced Materials Research*. **291-294**, 1748-1751. https://doi.org/10.4028/www.scientific.net/AMR.291-294.1748 (2011).
4. Li, W. C., Lin, Q., Ye, W. & Zhang, C. Y. Kinetics of rare-earth effect on the low carbon steel containing arsenic. *Journal of Beijing University of Iron and Steel Technology*. **2**, 61-67. https://dx.doi.org/10.13374/j.issn1001-053x.1983.02.025 (1983).
5. Du, T. Physical-chemistry effect of rare-earth elements on metallic material. *Act Metall Sin*. **33**, 69-77. https://www.ams.org.cn/EN/Y1997/V33/I1/69 (1997).
6. Cheng, H. J., Wang, F. M., Li, C. R., Tan, Y. P. & Wang, J. J. Effect of arsenic on microstructure and mechanical properties of 45 steel. *Heat Treatment of Metals* **35**, 33-38. (2010).
7. Zhang, F. Z. The Prospect of the Application of Rare-earth in Iron and Steel from the Phase Diagram of Rare-earth. *Iron Steel*. **8**, 66-75. (1986)
8. Brandes, E. A. & Brook. G. B. *Smithells Metals Reference Book*, Butterworth-Heinemann. (1983).
9. Yin, G. The distribution of arsenic in steel. *Gangtie*. **16**, 20-28. https://doi.org/10.13228/j.boyuan.issn0449-749x.1981.02.004 (1981).
10. Duan, S., Chen, X., Yang, B., Liu, D. & Dai, Y. Ab-Initio Molecular Dynamics Simulation of Thermal Decomposition of Arsenic-Iron Compounds in Vacuum. *Chin. J. Vac. Sci. Technol*. **34**, 1128-1134. https://doi.org/10.13922/j.cnki.cjovst.2014.10.23 (2014).
11. Hu, Q. Q., Zhou, J., Zhang, X. Y., Yan, Z. & Yang, Y. T. Comparison of As(V)Removal by Three Different Types of Ferric Iron Adsorbents. *Water Purif. Technol*. **33**, 71-74. https://doi.org/10.15890/j.cnki.jsjs.2014.06.013 (2014).
12. Todorov, I., Chuang, D., Malliakas, C., Li, Q., Bakas, T. & Douvalis, A. *et al*. $CaFe_4As_3$: A metallic iron arsenide with anisotropic magnetic and charge-transport properties. *Journal of the American Chemical Society*. **131**, 5405. https://doi.org/10.1021/ja900534h (2009).
13. Stoyko, S. S., Blanchard, P. E. R & Mar, A. Ternary rare-earth iron arsenide $RE_{12}Fe_{57.5}As_{41}$(RE=La, Ce). *Inorganic Chemistry*. **49**, 2325-2333. https://doi.org/10.1021/ic902231b (2010).
14. Zhang, J. Z. & Dou, S. T. Study on Interaction between Cerium and Arsenic. *Advanced Materials Research*. **194**, 1231-1234. https://doi.org/10.4028/www.scientific.net/AMR.194-196.1231 (2011).
15. Liu, X.; Zhang, J.; Zhu, S. Microstructure and compound Developed from La-As-Fe System at 1223K. *Advanced Materials Research*. **702**, 145-148. https://doi.org/10.4028/www.scientific.net/AMR.702.145 (2013).
16. Sklyarova, A., Tewari, G. C., J, Lindén., Mustonen, O., Rautama, E. L. & Karppinen, M. Mössbauer study of hyperfine interactions in $EuFe_2(As_{1-x}P_x)_2$ and $BaFe_2(As_{1-x}P_x)_2$. *Journal of Magnetism and Magnetic Materials*. **378**, 327-332. https://dx.doi.org/10.1016/j.jmmm.2014.11.054 (2015).
17. Munevar, J., Micklitz, H., Alzamora, M., Argüello, C., Goko, T. & Ning, F. L. *et al.* Magnetism in superconducting $EuFe_2As_{1.4}P_{0.6}$ single crystals studied by local probes. *Solid State Communications*. **187**, 18-22. https://doi.org/10.1016/j.ssc.2014.02.001 (2014).
18. Wu, T., Wu, G., Chen, H., Xie, Y. L., Liu, R. H. & Wang, X. F. *et al*. Magnetic phase diagram of $Eu_{1-x}La_xFe_2As_2$ single crystals. *Journal of Magnetism and Magnetic Materials*. **321**, 3870-3874. https://dx.doi.org/10.1016/j.jmmm.2009.07.043 (2009).

19. Terashima, T., Suzuki, H. S., Tomita, M., Kimata, M., Satsukawa, H. & Harada, A. *et al*. Pressure-induced antiferromagnetic bulk superconductor $EuFe_2As_2$. *Physica C Superconductivity*. **470**, S443-S444. https://doi.org/10.1016/j.physc.2009.10.064 (2010).
20. Drief, F., Zaoui, A., Kacimi, S. & Merabet, B. Ab-initio investigation of the electronic structure in the superconducting $EuFe_2(As_{1-x}P_x)_2$. *Physica C: Superconductivity and its Applications*. **512**, 22-27. https://doi.org/10.1016/j.physc.2015.02.045 (2015)
21. Xie, W. H., Huang, R., Zhang, J. Z., Li, W., Yang, Y. Study on the interaction of rare earth element neodymium, iron and arsenic at 1173 K. *Journal of Function Materials*. **49**, 1134-1138. (2018).
22. Fu, C. H., Huang, R., Xie, W. H., Luo, J. X. & Zhang, J. Z. Study on High-Temperature Interaction Mechanism of Nd-Fe-As System. *Materials*. **12**, 3060-. https://doi.org/10.3390/ma12193060 (2019).
23. Boi, B. I. & Lui, R. J. Diffusion in iron-arsenic alloys. *Journal of Materials Science*. **11**, 887-891. https://doi.org/10.1007/bf00542306 (1976).
24. Li, Y. L, Huang, R.; Yang, Y., Luo, J. X., Fu, C. H. & Zhang, J. Z. High-temperature interaction of Ce-Fe-As ternary system. *Materials Research Express*. **6**. https://doi.org/10.1088/2053-1591/ab1198 (2019).
25. Bramfitt, B.L. The effect of carbide and nitride additions on the heterogeneous nucleation behavior of liquid iron. *Metallurgical Transactions*. **1**, 1987–1995. https://doi.org/10.1007/BF02642799 (1970).
26. Villars, P. Pauling file. In Inorganic Solid Phases, *SpringerMaterials (Online Database)*; Springer: Heidelberg, Germany, (2012).

Acknowledgements
This research was funded by the Nation Natural Science Foundation of China (Grant No. 51664003 and 52064010).

Author Contributions
R.H. conceived and designed the experiment; C.F., L.X., and L.H. contributed to retrieve documents; J.M. collected the data and made the graph; J.M. analyzed the data and wrote the paper. This article was checked and revised by J.Z. All authors reviewed the manuscript.

Competing interests
The authors declare no competing interests.

Additional information
Correspondence and requests for materials should be addressed to R.H. or J.Z
Reprints and permissions information is available at www.nature.com/reprints.
Publisher's note Springer Nature remains neutral with regard to jurisdictional claims in published maps and institutional affiliations.

Figures

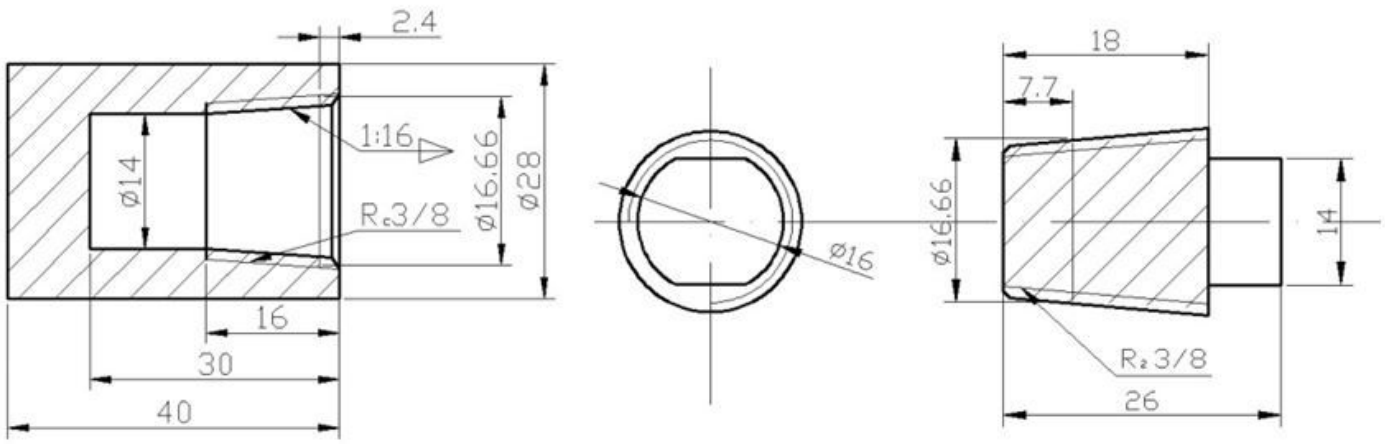

Figure 1

Schematic of the barrel-shaped cylinder and the screw plug.

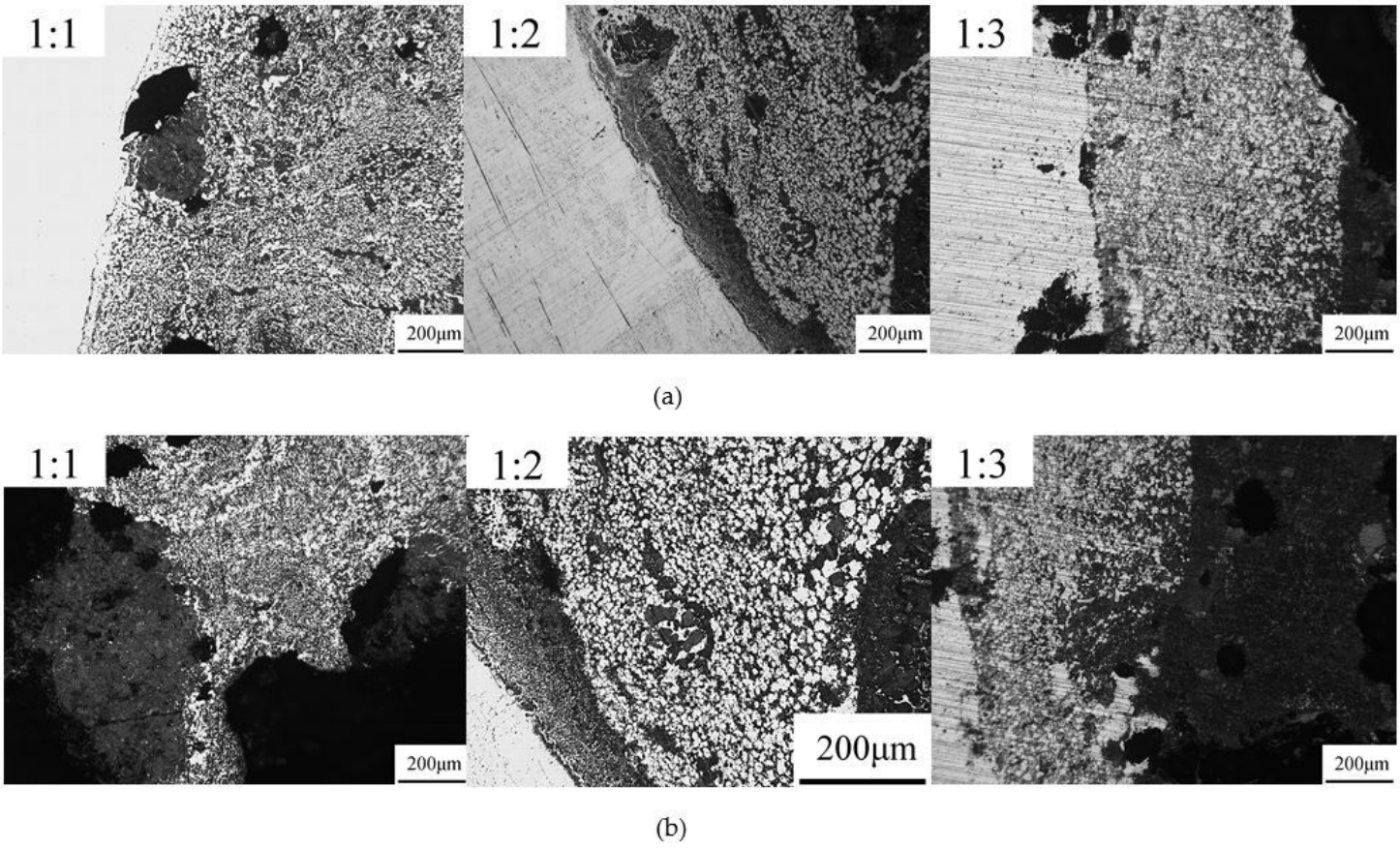

Figure 2

Metallographic pictures of atoms at different atomic ratio, (a) Pictures of the cylinder block's neighboring area, (b) Pictures around its core area.

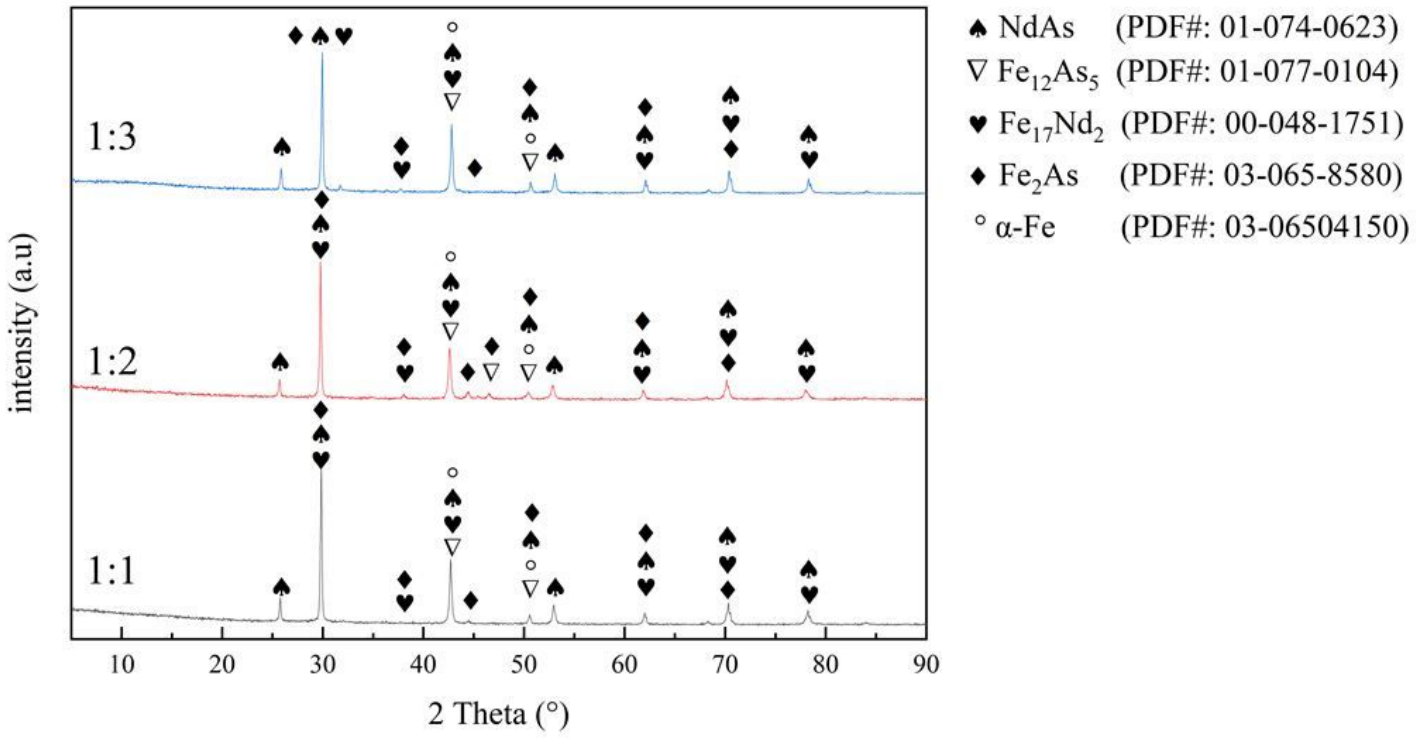

Figure 3

X-ray diffraction spectra of the samples at different atomic ratio.

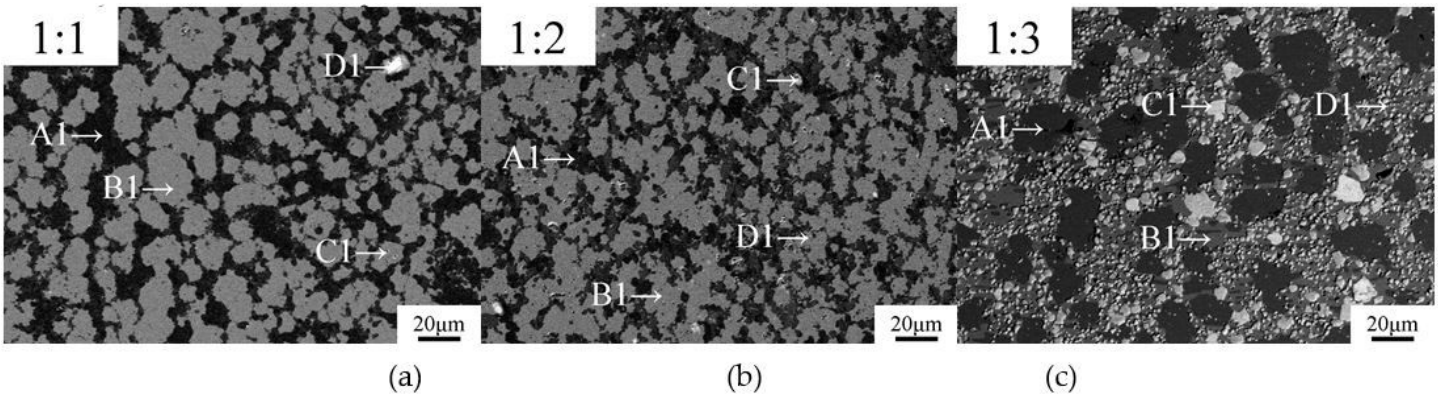

Figure 4

Backscattered electron maps of the sample at various atomic ratios (a) 1:1, (b) 1:2, (c) 1:3.

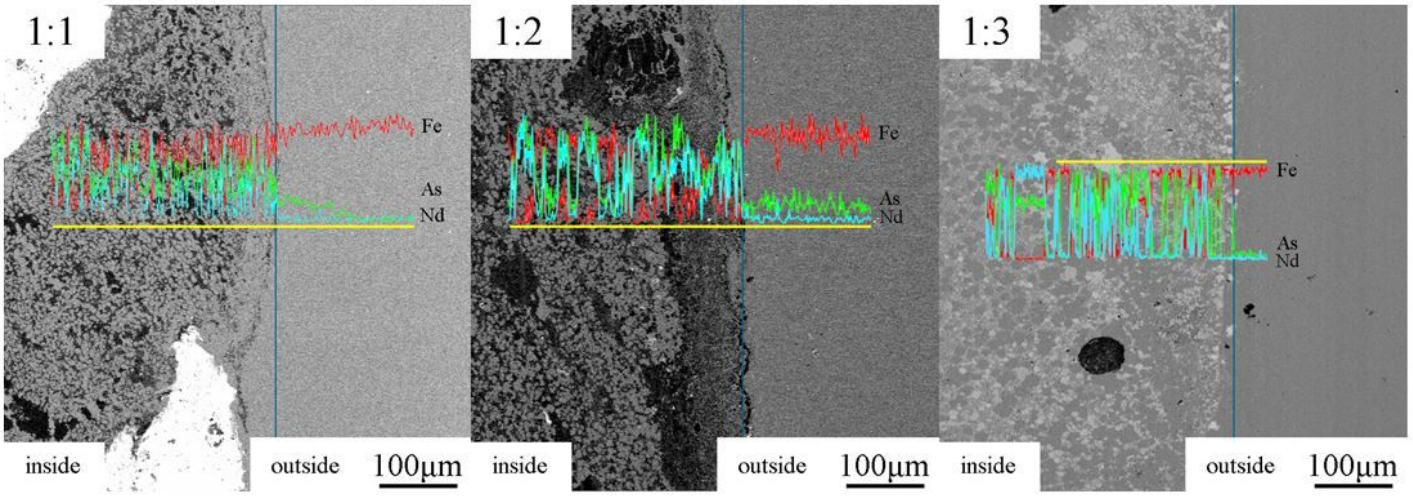

Figure 5

Sweep spectrum of the edge line of the cylinder samples at different atomic ratio.

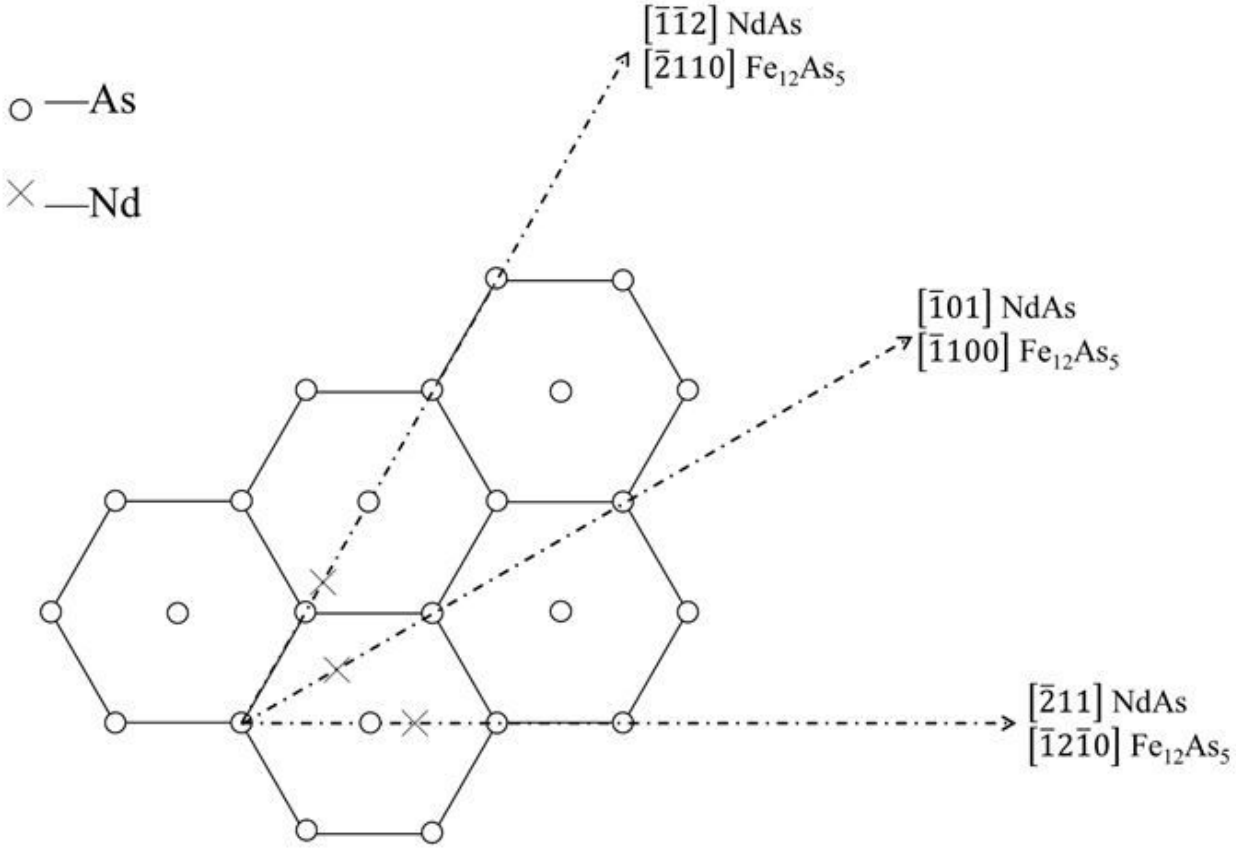

Figure 6

Crystallographic relationships of the Fe12As5 (0001) and NdAs (111) planes.

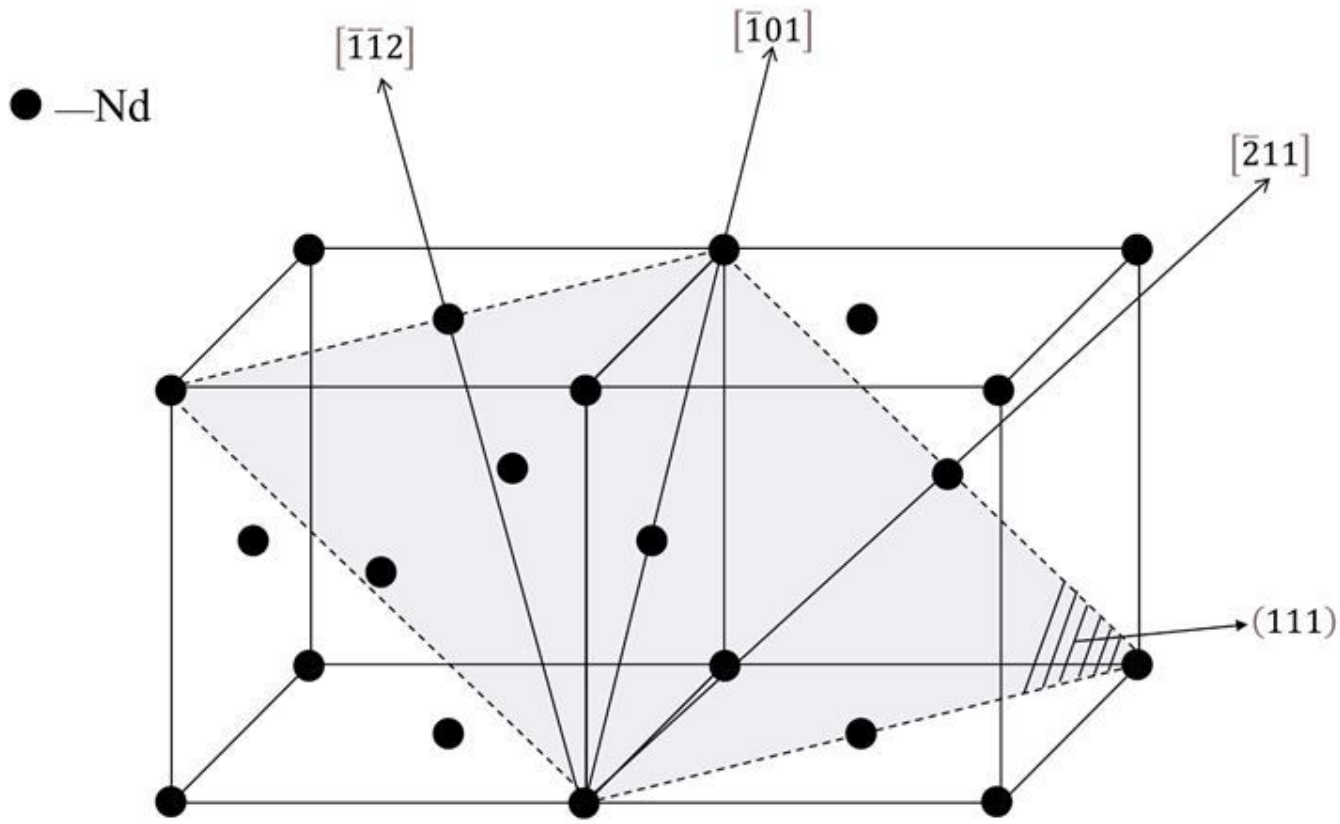

Figure 7

Diagram of plane and crystal direction of NdAs (111).